Merger-induced metallicity dilution in cosmological galaxy formation simulations

Sebastián Bustamante,[1]★ Martin Sparre,[2,3,4] Volker Springel[1,5,6] and Robert J. J. Grand[1,5]

[1]*Heidelberger Institut für Theoretische Studien, Schloss-Wolfsbrunnenweg 35, D-69118 Heidelberg, Germany*
[2]*Institut für Physik und Astronomie, Universität Potsdam, Karl-Liebknecht-Str, 24/25, D-14476 Golm, Germany*
[3]*Leibniz-Institut für Astrophysik Potsdam (AIP), An der Sternwarte 16, D-14482 Potsdam, Germany*
[4]*Department of Physics, Kavli Institute for Astrophysics and Space Research, MIT, Cambridge, MA 02139, USA*
[5]*Zentrum für Astronomie der Universität Heidelberg, Astronomisches Recheninstitut, Mönchhofstr, 12-14, D-69120, Heidelberg, Germany*
[6]*Max-Planck-Institut für Astrophysik, Karl-Schwarzschild-Str, 1, D-85741 Garching, Germany*

ABSTRACT

Observational studies have revealed that galaxy pairs tend to have lower gas-phase metallicity than isolated galaxies. This metallicity deficiency can be caused by inflows of low-metallicity gas due to the tidal forces and gravitational torques associated with galaxy mergers, diluting the metal content of the central region. In this work we demonstrate that such metallicity dilution occurs in state-of-the-art cosmological simulations of galaxy formation. We find that the dilution is typically 0.1 dex for major mergers, and is noticeable at projected separations smaller than 40 kpc. For minor mergers the metallicity dilution is still present, even though the amplitude is significantly smaller. Consistent with previous analysis of observed galaxies we find that mergers are outliers from the *fundamental metallicity relation*, with deviations being larger than expected for a Gaussian distribution of residuals. Our large sample of mergers within full cosmological simulations also makes it possible to estimate how the star formation rate enhancement and gas consumption timescale behave as a function of the merger mass ratio. We confirm that strong starbursts are likely to occur in major mergers, but they can also arise in minor mergers if more than two galaxies are participating in the interaction, a scenario that has largely been ignored in previous work based on idealised isolated merger simulations.

Key words: methods: numerical – galaxies: interactions – galaxies: star formation – galaxies: evolution.

1 INTRODUCTION

The interstellar medium (ISM) in galaxies is steadily enriched by heavy elements formed during the life and death of stars. This enrichment is accompanied by accretion of low-metallicity gas from reservoirs surrounding galaxies. Observations yield a correlation between the stellar mass ($M_\star$) and the metallicity of the star-forming gas (Z_{gas}) of galaxies (Tremonti et al. 2004). The existence of this correlation shows that the heavy chemical elements of a galaxy are – at least to first order – gradually built up during its lifetime. However, the relation has a significant scatter of 0.1 dex (Tremonti et al. 2004), indicating that galaxies evolve on diverse paths through the $M_\star - Z_{gas}$-plane.

A partial reason for the scatter in this relation is that galaxies with high star formation rates (SFR) at a fixed stellar mass usu-

ally have lower metallicities than galaxies with smaller SFR. This behaviour is encoded in the observation that galaxies evolve on a two-dimensional curved surface, dubbed the *fundamental metallicity relation* (FMR), in a three-dimensional space defined by the SFR, $M_\star$ and Z_{gas} of galaxies (Ellison et al. 2008a; Mannucci et al. 2010). While the presence of this relation has been confirmed by several studies (Lara-López et al. 2010; Belli et al. 2013; Stott et al. 2013; Yabe et al. 2015), it has, however, been questioned whether the FMR is *fundamental* (i.e. redshift-independent) because several observations at $z \sim 2.3$ reveal differences from the FMR in the local Universe (Salim et al. 2015; Brown, Martini & Andrews 2016; Grasshorn Gebhardt et al. 2016; Sanders et al. 2017, see also Christensen et al. 2012 for a study of $1 < z < 6$ lensed galaxies). Sanders et al. (2017) suggest that the redshift evolution of the FMR can be explained by an evolution of the mass-loading factor at fixed stellar mass, and by an evolution of the metallicity of infalling gas.

Even though the FMR might be redshift-dependent, it is interesting to ask what is driving its shape. A simple analytical model

★ E-mail: sebastian.bustamante@h-its.org

by Dayal, Ferrara & Dunlop (2013) explains the local FMR by accounting for star formation, inflow of metal-poor gas from the intergalactic medium, and outflow of gas from the interstellar medium. The FMR has also been reproduced in more sophisticated hydrodynamical galaxy formation models (Lagos et al. 2016; Davé et al. 2017; De Rossi et al. 2017; Torrey et al. 2017b).

Galaxy pairs are observed to have lower gas-phase metallicities and an increased SFR compared to isolated galaxies with comparable stellar masses (Ellison et al. 2008b; Scudder et al. 2012; Cortijo-Ferrero et al. 2017). They also show a flattening of the standard radial metallicity gradient in the case of spiral galaxies (Rupke, Kewley & Chien 2010; Kewley et al. 2010; Perez, Michel-Dansac & Tissera 2011). Qualitatively, this agrees well with the FMR, but a careful statistical study of SDSS galaxies shows that the FMR has an overabundance of outliers (compared to a Gaussian distribution of residuals), which might be caused by interacting galaxies with strong merger-induced gas inflows that dilute the metallicity and enhance the SFR (Grønnow, Finlator & Christensen 2015).

Given that observations can only probe a single instant in time of any individual merger, it is helpful to use simulations to establish how the metallicity dilution and SFR-enhancement in mergers occur. Remarkable insights have been gained about the metallicity evolution of mergers based on idealized simulations, where two equilibrium galaxies are set up to collide on a Keplerian orbit. Torrey et al. (2012a), for example, established that metallicity dilution is associated with nuclear inflows, and metallicity enhancement is caused by chemical enrichment from active star formation. Even though idealized merger simulations can give important hints on how a merger makes the gas migrate inwards and subsequently causes a starburst, it is important to keep in mind that such simulations are not cosmologically self-consistent. Cooling of hot gas onto the ISM (Moster et al. 2011), accretion of minor galaxies, and post-merger gas accretion (which proves to be important, e.g. Sparre & Springel 2017) are usually not included in idealized simulations. Properly accounting for these phenomena gives a more realistic view of how the metallicity dilution and SFR-enhancement occur in real galaxies.

In this paper, we study the metallicity dilution of galaxies in galaxy mergers based on a large set of high-resolution cosmological simulations. In addition to having realistic collision orbits and structures of the involved galaxies, using cosmological simulations also makes it possible to self-consistently study how the galaxy properties evolve before and after the merger under the influence of the surrounding gas reservoirs. We can use this to reveal for the first time how simulated mergers evolve relative to the FMR.

In Section 2, we present the Auriga simulations on which our analysis is based, and we briefly discuss the implemented physics model and the selection of our sample of mergers. In Section 3, we correlate both metal dilution and SFR-enhancement with the mass-ratio of the mergers. We also study how the metallicity dilution depends on the separation of the merging galaxies. In Section 4, we analyse how mergers behave relative to the FMR. Finally, we discuss our results and conclude in Sections 5 and 6, respectively.

2 SIMULATIONS AND SAMPLE SELECTION

2.1 Auriga simulations

The simulations studied in this paper are based on the Auriga project (Grand et al. 2017), which comprises a set of 30 cosmological magnetohydrodynamical zoom simulations of the formation of late-type isolated galaxies within Milky Way mass dark haloes. These haloes were extracted from a parent dark matter only simulation in a periodic cube of 100 comoving Mpc on a side from the EAGLE project (Schaye et al. 2015), and were selected to have a viral mass[1] in the range $10^{12} < M_{200}/M_\odot < 2 \times 10^{12}$, and to satisfy a mild isolation criterion at $z = 0$. However, no selection criteria were imposed at $z > 0$, therefore the merger histories are unconstrained and exhibit a variety of evolutionary paths. The simulations were carried out with the moving-mesh code AREPO (Springel 2010; Pakmor et al. 2016). A Planck-2014 ΛCDM cosmology (Planck Collaboration et al. 2014) was adopted, specified by $\Omega_m = 0.307$, $\Omega_b = 0.048$, $\Omega_\Lambda = 0.693$, and Hubble constant $H_0 = 100 \, h \, \mathrm{km \, s^{-1}}$, with $h = 0.6777$. We refer the reader to Grand et al. (2017) for a detailed and comprehensive description of the simulations.

2.2 Definition of the merger sample

To construct our global merger sample, we use the 30 Auriga simulations at resolution *level 4*.[2] Galaxies and merger trees are identified by standard methods (Rodriguez-Gomez et al. 2015; Springel et al. 2005). We define merger events as times when a galaxy has more than one direct progenitor and each progenitor has a stellar mass of at least 1 per cent the stellar mass of the main progenitor. This is done in order to avoid spurious effects introduced by unresolved objects. With these conditions, we obtain 137 mergers.

For each galaxy merger, we define the stellar mass-ratio, μ, as the mass of the secondary galaxy divided by that of the main progenitor. We determine the stellar masses at the time when the mass of the secondary galaxy reaches its local maximum before the merger. We define the merger ratio in such a way that we always have $\mu \leq 1$.

To characterize the mergers, we also calculate the *time of first pericentral passage*, t_{per}, and the *time of final coalescence*, t_{coal}. We define the latter as the peak time of the central black hole accretion rate, or the time at which the mean radial distance of the 10 most bound particles of the secondary progenitor reaches the half-mass radius of the main progenitor, whichever is later. As a caveat, due to the relatively sparse temporal frequency at which the snapshots of the simulations are stored, i.e. $\sim$100 Myr at the redshift range of our sample, all temporal quantities associated to the mergers have an intrinsic uncertainty of about this value.

We restrict ourselves to coalescence times corresponding to $z_{coal} \leq 1.5$, and we require the most massive galaxy in a merger to have at least $M_* \geq 10^{9.5} \, \mathrm{M_\odot}$. We briefly remind the reader that the limited $z = 0$ mass range of the Auriga galaxies sets an upper limit of $M_* \simeq 2 \times 10^{11} \, \mathrm{M_\odot}$ on our merging galaxies.

To create a master sample consisting only of *clean mergers*, from our global sample, we exclude those that have other mergers in a short timespan; we specifically require no other mergers with $\mu > 1 : 100$ to occur within 1 Gyr of the first pericentral passage and of final coalescence, i.e. in the time interval $t_{per} - 1 \, \mathrm{Gyr} < t < t_{coal} + 1 \, \mathrm{Gyr}$.

In a few instances, our merger tree method has problems to properly track the main progenitor. This happens when we have two galaxies of similar mass experiencing a fly-by, but no subsequent merger. In these cases, the merger tree algorithm may swap the assignment of being the main progenitor several times back and forth between the two galaxies. We exclude epochs from our sample where such progenitor swaps occur.

---

[1]Defined to be the mass inside a sphere in which the mean matter density is 200 times the critical density, $\rho_{crit} = 3H^2(z)/(8\pi G)$.
[2]In the nomenclature of Grand et al. (2017).

With these selection criteria, we obtain a master sample of 70 mergers, allowing us to statistically study the properties of mergers. To summarize, all these mergers occur at $z < 1.5$ and have masses of $10^{9.5}\,\mathrm{M}_\odot \leq M_* \leq 2 \times 10^{11}\,\mathrm{M}_\odot$. The total gas fractions of the mergers, defined relative to the total halo mass, range from 9 per cent to 16 per cent, meaning that they are typically gas-rich, and thus ideal to study the process of metallicity dilution.

2.3 A sample of isolated galaxies

In Section 4.1, we will compare our merger sample with isolated galaxies. We construct a suitable comparison sample by marking those Auriga galaxies as isolated where no mergers with $\mu \geq 1$: 100 occur within 1 Gyr. To be specific, we exclude all times within time-intervals, $t_{\mathrm{per}} - 1\,\mathrm{Gyr} < t < t_{\mathrm{coal}} + 1\,\mathrm{Gyr}$, of any $\mu \geq 1$: 100 merger.

2.4 Physics model

All simulations use the Auriga galaxy formation model, see Grand et al. (2017) for a comprehensive overview. As highlighted in Torrey et al. (2012a), there are four key processes that influence the evolution of metallicity and star formation in galaxies, namely nuclear inflows of low-metallicity gas, chemical enrichment from active star-forming regions, galactic outflows, and locking of gasphase metallicity in the stellar phase. Metallicity dilution and SFR-enhancement can therefore be understood as a consequence of the competition between these processes, where usually nuclear inflow and chemical enrichment dominate at low and high redshift, respectively. Below, we concisely describe how these different aspects are accounted for in the Auriga physics model (for more details, see Vogelsberger et al. 2013; Marinacci, Pakmor & Springel 2014; Grand et al. 2016).

For modelling the interstellar medium (ISM), the subgrid two-phase model first presented in Springel & Hernquist (2003) is implemented. In this, star-forming gas cells are considered to be composed of two different phases, namely a cold, dense phase embedded into a hot, diffuse ambient medium. Above a density threshold of $n = 0.13\,\mathrm{cm}^{-3}$, gas cells are assumed to enter a thermally unstable star-forming regime where, according to the Chabrier (2003) initial mass function, they are stochastically converted either into a star particle or a SNII feedback-induced wind particle launched in an isotropic direction. In the former case, the created star particle represents a single stellar population with a given age, mass, and metallicity. Metal enrichment and mass loss from SNIa (Thielemann et al. 2003; Travaglio et al. 2004) and AGB stars (Karakas 2010) are modelled by calculating how much mass per star particle moves off the main sequence at every time step. The returned metals and gas mass are then deposited into nearby gas cells with a top-hat kernel.

Note that the implemented gas-recycling approach is drastically different from the stochastic approach presented in Torrey et al. (2012a), where a star particle has a probability to become an SPH gas particle depending on a characteristic recycling time-scale. Although their approach gives a less accurate tracking of the spatial and temporal distribution of metals and mass, it allows the tracing of the origin of any particular mass or metal element, thereby allowing to differentiate enriched metals from an initially set metallicity profile. In our case of cosmological simulations, all the metal content is produced from star formation enrichment within the simulation. The wind particles are launched with a metal content determined by the initial gas-phase metallicity, and are re-coupled to the gas once

they reach a gas cell with a density below 0.05 times the density threshold for star formation or a maximum travel time is exceeded. In either of these cases, their metal, mass, momentum, and energy contents are deposited into the local gas cell. This ensures that the wind material leaves its launching site, favouring the production of gas outflows in the simulation.

Additionally, we include prescriptions for a uniform background UV field for reionization (completed at $z = 6$), primordial and metal line cooling, magnetic fields, as well as subgrid models for black hole seeding, growth through accretion, and associated feedback.

3 METALLICITY DILUTION AND STARBURST PROPERTIES

To introduce the concept of metallicity dilution, we show the evolution of the SFR-weighted gas-phase metallicity of the primary galaxy of one of the major mergers in our sample in Fig. 1. Note that we use SFR-averaged metallicities to mimic observations of HII regions of star-forming gas. The projections in Fig. 1 are done onto the galactic plane for three different zoom levels of 200, 40, and 8 kpc. In the analysis, we adopt a solar metallicity of $Z_\odot = 0.02$. For the first two snapshots, shown in the first and second columns, we see that the metallicity profile does not change appreciably, and it is only when the secondary galaxy comes closer than 40 kpc that the metallicity gets significantly diluted, as seen at the coalescence time in the third column (see also *merger 1* in Fig. 2). In the fourth column, 0.28 Gyr after the merger, the enhanced SFR replenishes the metal content of the gas in the central region through stellar enrichment, defining thus the end of the dilution period. In the following, we study the dilution process in galaxy mergers in more detail.

3.1 Time evolution

To introduce the primary quantities we use in our analysis, we plot the evolution of four different mergers from our sample in Fig. 2. These mergers are selected as representative cases for major mergers (defined to have $\mu > 1/3$, which is also the same criterion used to select major mergers, e.g. in Lotz et al. 2008).

In order to quantify the behaviour of metallicity dilution and SFR-enhancement during a merger, we analyse the nuclear region of the main progenitor. We define the nuclear region to be a sphere of radius 2 kpc around the galactic centre (identified with the minimum of the galactic gravitational potential). This cut is chosen to mimic the effect of a limited aperture of an SDSS fibre. For each snapshot, we define the SFR-averaged metallicity as

$$Z_{\mathrm{gas}} = \frac{\sum_i \mathrm{SFR}_i\, Z_i}{\sum_i \mathrm{SFR}_i}, \tag{1}$$

where i runs over all gas cells inside the nuclear region, SFR_i and Z_i are the instantaneous star formation rate and the fraction of gas mass in metals in the ith gas cell, respectively.

In the first row in Fig. 2, the gas-phase metallicity has been calculated based on the gas cells inside the galaxy corresponding to the main branch of the merger tree, as a function of time. The evolution of Z_{gas} reveals that these galaxies experience a dilution of metallicity right before or at the time of the SFR peak. To quantify the metallicity dilution, we define the pre-merger background metallicity level as the previous local maximum prior to the time when the metallicity minimum occurs. We refer to the time where we determine the background metallicity as $t_{Z_{\mathrm{max}}}$. In the plot, the background and minimum metallicity levels are marked as the ends
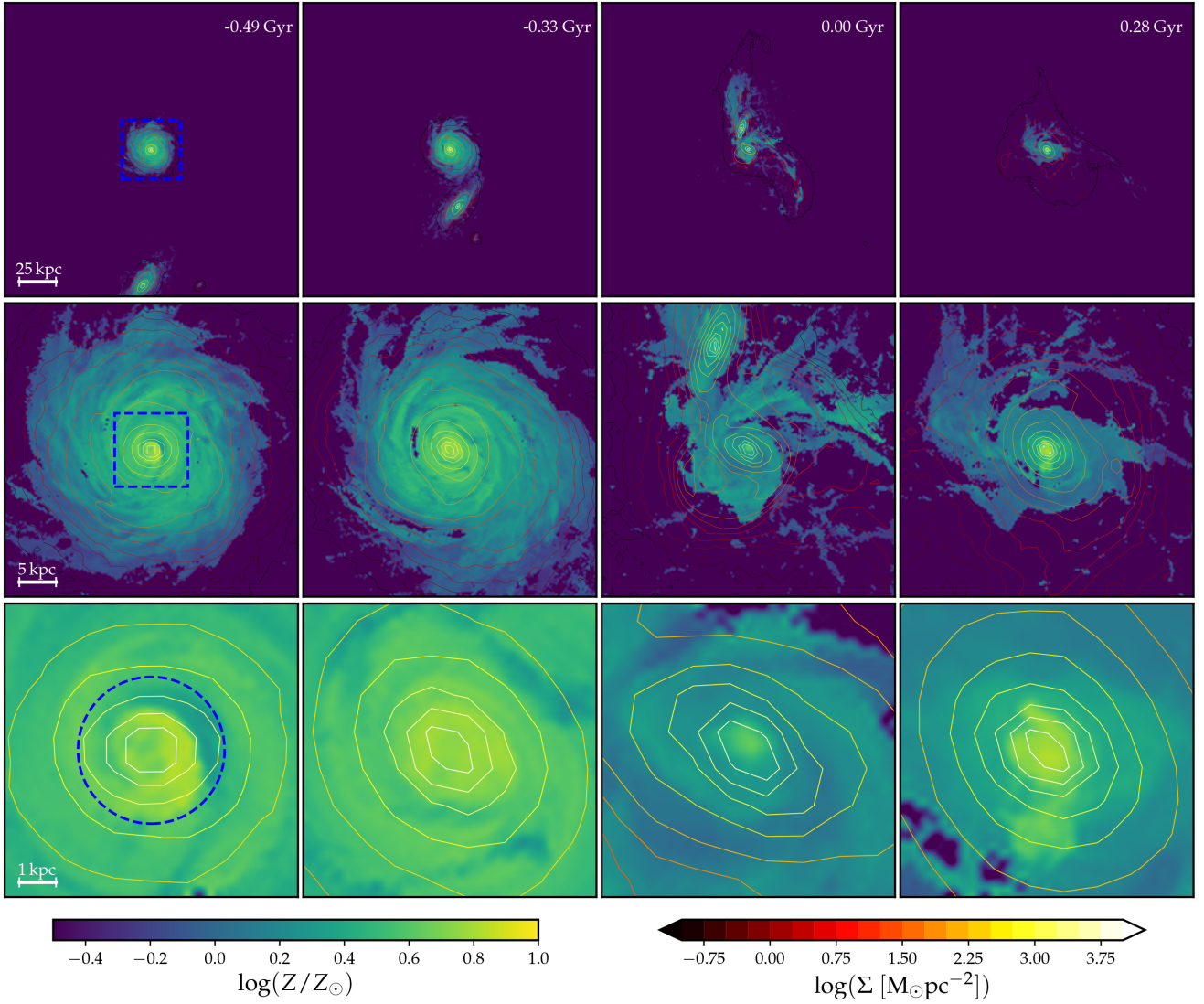
Figure 1. Projection of the SFR-weighted gas-phase metallicity (colour map) and stellar surface density (colour contours) of the primary galaxy in *merger 1*. From left to right, we show four different snapshots of the evolution, corresponding to −0.49, −0.33, 0, and 0.28 Gyr. From top to bottom, we show different zoom levels with 200, 40, and 8 kpc on a side, respectively. For the first and second rows, the white dashed-line squares enclose the region shown in the next zoom level. For the third row, the white dashed-line circles correspond to the central 2 kpc-radius region for which we calculate all the studied properties. The metallicity in the nuclear region reaches its lowest value close to the coalescence time ($t = 0$ Gyr), when the gas inflow is strong. Furthermore, we note that outside this region, there is also a somewhat weaker dilution, indicating that the dilution process extends across the galactic disc. In the post-merger stage, the metallicity increases again in an inside-out way.

of the dashed vertical lines, which represent the metallicity dilution times. Based on the ratio of these two levels, we define $\Delta \log Z_{\mathrm{gas}}$, which we will refer to as the metallicity dilution.

The second row shows the SFR, which is calculated in the same fashion as the metallicity. The SFR peaks, marked by dashed vertical lines, are determined as the largest SFR-value of the main progenitor within 1 Gyr of the merging time registered in our merger trees. To determine the fractional increase in SFR due to the merger-induced starbursts, we measure the pre-merger background SFR-level by applying a smoothing algorithm to filter out short timescale fluctuations over 1 Gyr. Then, we find the local minimum before the SFR peak. The background SFR-level is determined as the corresponding value in the original non-smoothed profile, and the time at which this occurs defines $t_{\mathrm{SFR_{min}}}$. The fractional SFR-enhancement is then calculated as the ratio between the peak SFR and the background

level. In the remaining parts of the paper, we will use $\Delta \log \mathrm{SFR} \equiv \log [\mathrm{SFR(peak)}/\mathrm{SFR(background)}]$ to quantify this fractional enhancement.

We see that the two strongest fractional metallicity dilutions occur in *merger 1* and *merger 4*. For *merger 2* and *merger 3*, we see a somewhat weaker dilution. Establishing the presence of metallicity dilution in cosmological simulations is a notable result, since this has so far mainly been studied in idealized merger simulations. The only other work that has found this effect in a cosmological simulation is Torrey et al. 2017b (see the left-hand panel of their Fig. 9), who identified a merger-induced epoch of metallicity dilution in a $M_* = 10^9 M_\odot$ galaxy.

The third rows show the ISM gas consumption time-scale, calculated as the ratio of the ISM gas mass (M_{ISM}, calculated using equation 1 from Torrey et al. 2012b) and the SFR of the galaxy. We
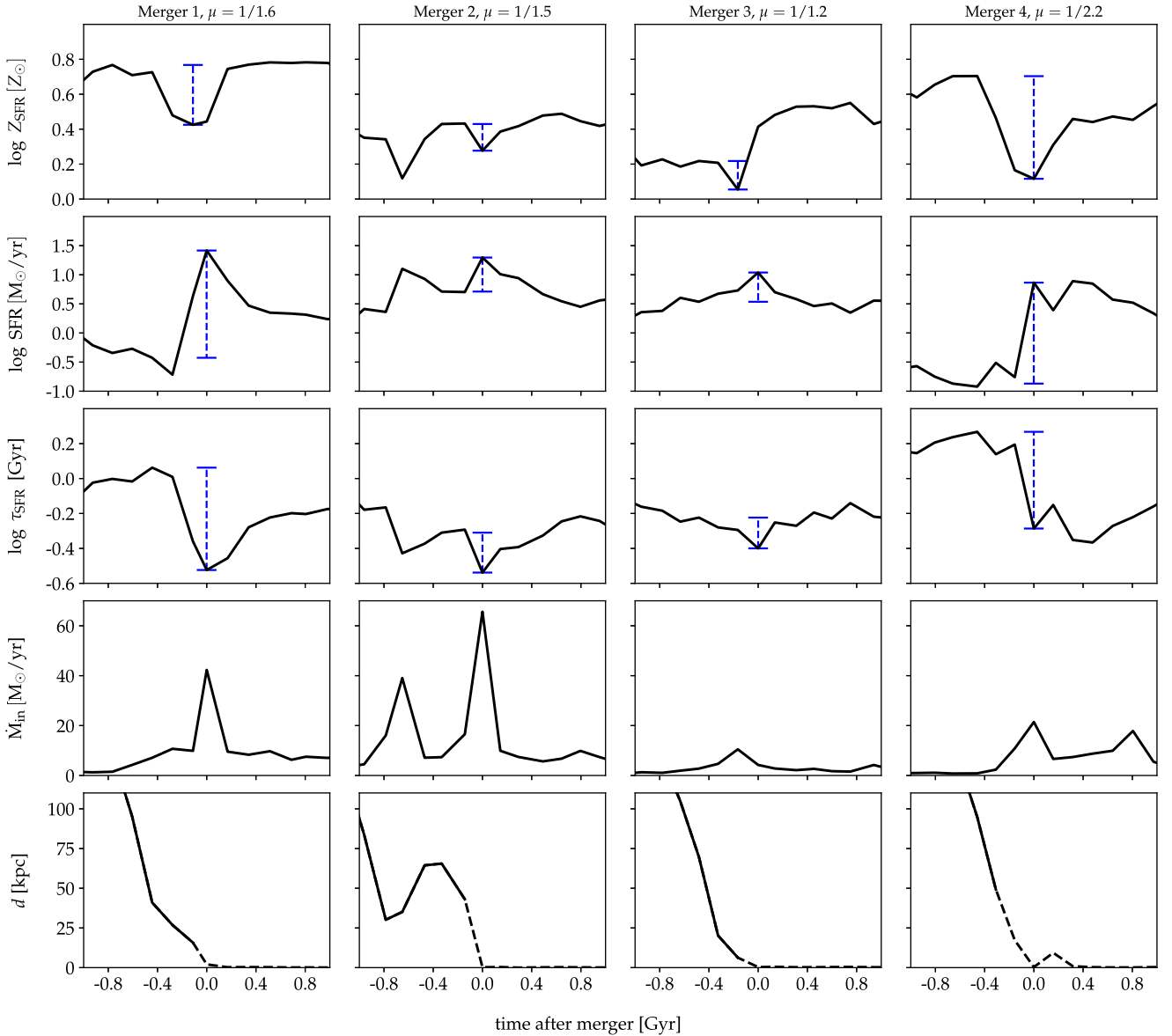
Figure 2. We show four typical major mergers, each presented in a separate column headed by the mass ratio. From top to bottom, we show the time-evolution of the gas metallicity inside 2 kpc (first row), the SFR (second row), the gas consumption timescale (third row), and the nuclear gas inflow rate (fourth row). We also show the radial distance between the two galaxies (fifth row), where dashed lines correspond to a reconstruction of the orbit based on the most bounded particles of the secondary galaxy after both galaxies have fused in the merger trees. The *x*-axis shows the time elapsed since t_{coal}, with negative values corresponding to pre-coalescence stages. In the first three rows, vertical dashed lines correspond to the fractional changes of the respective quantities. We see that these major mergers of our sample cause a significant metallicity dilution (especially for *merger 1* and *merger 4*), strong SFR-peaks, and a decrease in the gas consumption time-scale, demonstrating that those mergers form stars in a more bursty mode.

calculate this based on the ISM-gas-cells of the primary galaxy. The evolution of the gas consumption time-scale reveals that merger-induced starbursts are typically associated with a decrease in the ISM gas consumption time-scale, quantified in a similar fashion as for the gas-phase metallicity dilution, i.e. as the logarithm of the ratio between the nearest local minimum to the SFR-peak and the pre-merger local maximum $\Delta \log \tau_{SFR}$. This behaviour is also identified in the merger simulations of Sparre & Springel (2016), which uses the same physical galaxy formation model as the present paper. A decrease in τ_{SFR} shows that star formation occurs in a more bursty mode than for normal star-forming galaxies. A similar bursty mode is observed in galaxy mergers and ULIRGS (Sanders, Scoville &

Soifer 1991; Daddi et al. 2010; Krumholz, Dekel & McKee 2012; Scoville 2013).

Additionally, we show the nuclear gas inflow rate and relative radial distance (fourth and fifth rows, respectively). Note that all SFR-peaks and metallicity dilutions are accompanied by a conspicuous increase in the nuclear gas inflow, supporting thus the scenario where infalling pristine gas disrupted during the merger is the main driving mechanism of the dilution. The post-merger gas-phase metallicity level can vary widely from galaxy to galaxy depending on the infalling gas supply. For example, for *merger 1* and *merger 2*, the post-merger levels are similar to their pre-merger values owing to comparable pre- and post-merger gas supplies. In

merger 3, the gas supply is not enough to counteract enrichment from recently formed stars, and the post-merger metallicity is thus much larger than the pre-merger value. The opposite case occurs in *merger 4*, where a continuous post-merger gas supply keeps diluting the metallicity.

3.2 Correlations

Having shown that four of our mergers in subSection 3.1 have a strong SFR-peak associated with a decrease in the gas consumption time-scale and the nuclear metallicity, we will now study the behaviour of these quantities in our full merger sample. In order to do so, we show how $\Delta \log SFR$, $\Delta \log Z_{gas}$ and $\Delta \log \tau_{SFR}$ correlate with μ in Fig. 3.

First, we see that the strongest SFR-enhancements occur in mergers with large merger ratios. For example, the three highest values of $\Delta \log SFR$ occur in galaxies with $\mu > 0.5$. This is in good agreement with other studies showing that major mergers cause strong starbursts (Mihos & Hernquist 1996; Barnes 2004; Springel, Di Matteo & Hernquist 2005; Hayward et al. 2014). Specifically, the range of our relative SFR-enhancements for major mergers is in good agreement with what is typically found in idealized simulations (Martig & Bournaud 2008; Di Matteo et al. 2008; Teyssier, Chapon & Bournaud 2010; Hopkins et al. 2013; Karman et al. 2015; Moreno et al. 2015; Gabor et al. 2016).

For low-merger mass-ratios of $1/30 < \mu < 1/3$, there are a few mergers with relatively large SFR-enhancement of around 1.0 dex. Further inspection shows that while the merger goes on, there is another galaxy on its first passage around the main galaxy of the merger. The time between coalescence of the two galaxies, which are about to merge with the main galaxy, is more than 1 Gyr, which is why these galaxies have not been filtered out by our selection criteria for mergers to be *clean*. We have marked all these merging systems, which are affected by a third galaxy, with a square in the figure. The presence of systems where more than two galaxies are participating in the merger is a clear consequence of our use of cosmological simulations, where mergers do not occur in isolation. An interesting conclusion is that a minor merger – if we include the full cosmological structure in the surroundings including other galaxies – can trigger a star formation enhancement which is comparable to a major merger. This is not the first time such systems of multiple interacting galaxies are reported. For example, one of the systems (1349-3) from the simulations of Sparre & Springel (2016) also consists of multiple merging galaxies, and the observations of Stephan's Quintet also reveal such a system. Even though such systems of multiple interacting galaxies are expected to occur in the real Universe, they have, however, been largely overlooked in previous generation's of idealized modelling of merging galaxies.

On average, minor mergers with $\mu \simeq 0.1$ cause substantial SFR-enhancements of about 0.5 dex (a factor of 3). For lower merger ratios of $\mu < 0.05$, the SFR-enhancements are more modest, in most cases lower than a factor of 2. In idealized simulations, Cox et al. (2008) found the same conclusions; their merger with $\mu = 0.02$ causes an almost negligible SFR-peak, whereas their $\mu = 0.1$ merger causes a more visible – but still small – SFR-enhancement.

For the metallicity, the strength of the dilution increases gradually until $\mu \sim 1$, where the peak dilution is around 0.17 dex. We thus confirm the idealized simulations from Torrey et al. (2012a), which also show that metallicity dilution occurs in the centre of galaxies. The magnitude of the dilution in our work is slightly larger than the maximum dilution of $\sim$0.05 dex observed in Scudder et al. (2012) for galaxies being $\sim$11 kpc apart. However, there are sev-
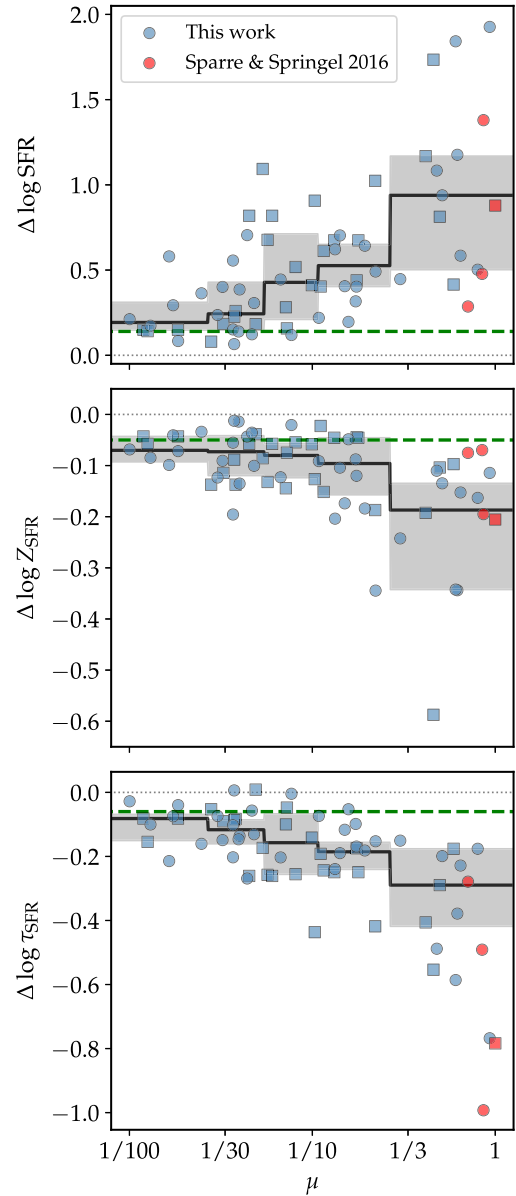

Figure 3. Dependence of the fractional enhancement/dilution of SFR (top panel), metallicity (middle panel), and gas depletion timescale (bottom panel) on the merger mass-ratio (μ). Solid lines correspond to median values, and grey regions to 25–75 per cent percentiles. The squares show galaxies where the merging pair is gravitationally affected by a third galaxy nearby (see text for details), and the circles show mergers where no other galaxies are nearby. All the properties exhibit a gradually increasing dependence on merger ratio. If we only take into account galaxies without a nearby third galaxy these results are consistent with previous idealised simulations of mergers, where $\mu > 1/3$ mergers can cause strong starbursts and $\mu < 1/3$ mergers cause more modest starbursts. A full inclusion of the cosmological environment, such as in the form of additional galaxies in the vicinity of the merger, can, however, significantly increase the SFR and decrease the gas depletion timescale of minor mergers.

eral possible explanations for this discrepancy: first, their selection criteria for galaxy pairs do not guarantee that these systems are strictly interacting galaxies; therefore, when non-interacting systems are included, the real extent of the metallicity dilution would be likely underestimated. Second, we are reporting values near to or

at the coalescence time, when the dilution is supposedly strongest.[3] This time corresponds to small projected distances $\lesssim 5$ kpc, which are more challenging to probe observationally. Finally, due to their weaker dilutions, they do not split the metallicity offsets into different merger ratio bins, even including merger ratios above one, i.e. they also use the secondary galaxies. When we do the same, we obtain a more modest median metallicity dilution of 0.08 dex, which is in better agreement. Overall, establishing the presence of metallicity dilution in cosmological simulations is an interesting finding as it shows that tidal forces and gravity torques exerted during more realistic mergers are mechanisms capable of driving enough nuclear gas inflows to produce metallicity dilution and SFR-enhancement, even in minor mergers, albeit at a lesser extent.

Epochs of very strong gas compression mostly appear when the merger ratios are high, see the median curve in the $(\mu, \Delta \log \tau_{\mathrm{SFR}})$-plot. A similar bursty mode for major mergers is also found in the hydrodynamical simulations of Renaud et al. (2014) and Sparre & Springel (2016).

The same plot also shows that $\mu \simeq 0.3$ is a characteristic scale above which the average τ_{SFR}-value experiences a decrease of ~ 0.3 dex (a factor of 2) during a merger. Moreover, four of the mergers in the same range (~ 30 per cent) exhibit even larger decreases of 0.5 dex up to 0.8 dex. Therefore, using $\mu \simeq 0.3$ as a threshold to distinguish major and minor mergers captures whether bursty epochs with short τ_{SFR}-values are likely to occur.

Finally, we quantify the fluctuations of SFR, metallicity, and depletion time-scale in isolated galaxies. In order to do so, we have implemented the same algorithm used for finding the peaks and dips associated to SFR-enhancements and metallicity dilution in mergers. For example, in the case of SFR, we find all the local maxima of a galaxy whenever it is marked as isolated according to our merger selection criteria. Then, for each maximum, we find the local minimum that occurs right before the time of the maximum. With these two values we quantify the fractional change of the fluctuation. For metallicity and depletion time-scale, we apply an analogous procedure. We show in every panel the mean value of the fractional change of these fluctuations as green dashed lines. Mergers with small stellar mass ratios (i.e. $\mu < 1/30$) exhibit fractional changes comparable to the fluctuation levels of isolated galaxies, which is consistent with the idea of very minor mergers not driving gas inward.

3.3 Projected distance

In Fig. 4 we have determined the SFR, the metallicity, and the projected distance as the merging galaxies from our sample approach each other for three different mass ratio bins. The projected distance corresponds to the projection on the *XY* plane of the merger orbit, which means that we assume only one viewing direction per merger. Metallicity dilutions and SFR-enhancements are measured relative to the pre-merger values at $t_{Z_{\max}}$ and $t_{\mathrm{SFR}_{\min}}$, respectively. Since we only have snapshots of our galaxies at a relatively sparse temporal frequency, it is not always the case that each galaxy merger is represented in every radial bin. In such a case, these galaxy mergers get a vanishing weight in those bins. Furthermore, a few mergers exhibit more complex orbits, causing their trajectories to be counted more than once in some radial bins. We evenly distribute the weights of multiple points of a given galaxy within a radial bin such that the sum of the weights is one. The final median profile is obtained by
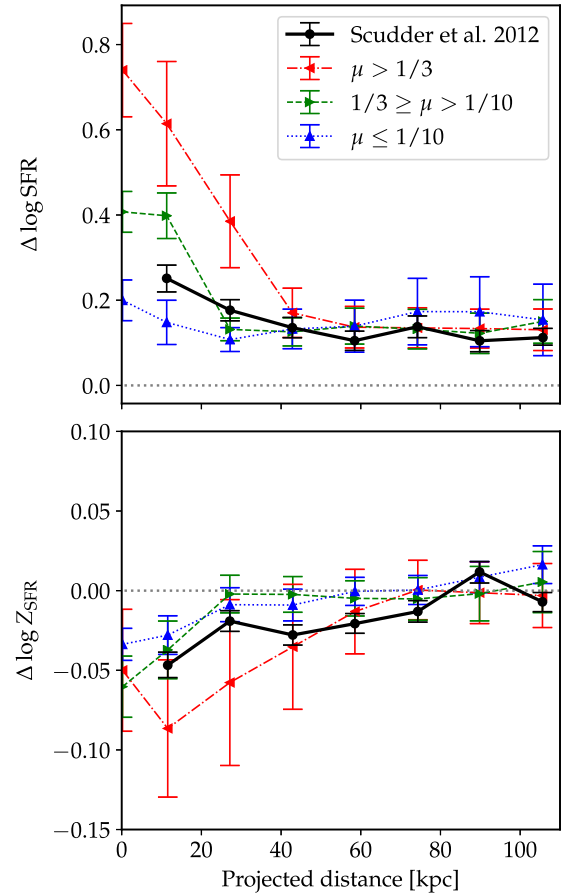
[3] Major mergers seem to be an exception to this. See Fig. 4.

Figure 4. Fractional change of the SFR (top panel) and the metallicity (bottom panel) as a function of projected distance for our sample of galaxies (dashed lines) and the observations of Scudder et al. 2012 (solid lines). The error bars show the standard error of the median. The observed sample shows SFR-enhancement at $r < 40$ kpc and metallicity dilution at $r < 60$ kpc. For our simulated sample, major mergers show SFR-enhancement at $r < 30$ kpc and dilution at $r < 40$ kpc. For minor mergers, SFR-enhancement and dilution occur at the same distances, within $r < 30$ kpc. The fractional changes are progressively stronger for larger mass ratios and smaller distances, with the exception of major mergers, where the dilution peak occurs at a distance ~ 10 kpc, which is slightly increasing with the coalescence time. This is caused by stellar metal enrichment overcoming the dilution.

stacking all the trajectories with the proper weights in every radial bin. Besides, we include data points at $r = 0$ corresponding to values at the coalescence time. Finally, to simplify comparison with the results reported by Scudder et al. (2012), our error bars also correspond to the standard error of the median.

The fractional changes near coalescence are stronger for larger mass ratios. For major mergers, the SFR-enhancement becomes significant at projected distances $r < 30$ kpc, whereas the metallicity dilution becomes noticeable at slightly larger distances $r < 40$ kpc. This difference is caused by merger-induced gas inflows diluting first the metals, and soon after producing a strong SFR-enhancement as a result of gas compression in the galactic centre. The magnitude of this process is also revealed by the slight increase of the metallicity at the coalescence time, caused by stellar metal enrichment starting to overcome the dilution. For minor mergers, both effects become significant at comparatively smaller distances, for $r < 20$ kpc. A smaller distance of influence is expected from the modest gravitational influence of smaller galaxies. Due to weaker

gas inflows in this case, the SFR-enhancement and the metallicity dilution sync up, with stellar metal enrichment overcoming the dilution only after coalescence.

Finally, we compare with the observations of Scudder et al. (2012). At large projected distances, the SFR-enhancements exhibit a similar behaviour, although their metallicity dilution is lower than ours. The reason for the differences is probably the different adopted normalizations. While they use a carefully selected control sample from which the fractional changes are calculated, we use pre-merger values due to our limited number of galaxies. At smaller distances, their values sit between our major and minor mergers, consistent with the mixed merger ratios in the sample that they use. Taking these considerations into account, we regard our simulations as consistent with the Scudder et al. (2012) observations. Our results also agree with the idealiszed simulations of Patton et al. (2013), who reproduced the observed trend from Scudder et al. (2012).

4 MERGERS AND THE FUNDAMENTAL METALLICITY RELATION

In this section, we characterize how mergers are positioned relative to the fundamental metallicity relation (FMR). In order to do so, we show in the left-hand panel of Fig. 5 the three-dimensional distribution of 1577 data points representing our galaxies in both isolated and merging phases. For each simulation, we study all galaxies in 60 snapshots logarithmically distributed in the redshift range $0 \leq z \leq 1.5$. The blue wireframe corresponds to a second-order polynomial in $M_\star$ and SFR fitted to the metallicity values, yielding:

$$\log(Z_{\mathrm{gas}})_{\mathrm{FMR}} = 0.471 + 0.549\,m - 0.214\,s - 0.099\,m^2$$
$$+ 0.010\,m\,s + 0.007\,s^2, \qquad (2)$$

where $m \equiv \log(M_\star) - 10$ and $s \equiv \log(\mathrm{SFR})$, with Z_{gas}, $M_\star$ and SFR in units of $Z_\odot$, $M_\odot$ and $M_\odot\,\mathrm{yr}^{-1}$, respectively. With the aim of testing the goodness-of-fit of this model, in the bottom panel of Fig. 5 we calculate the histogram of residuals $r \equiv \log(Z_{\mathrm{gas}})_{\mathrm{data}} - \log(Z_{\mathrm{gas}})_{\mathrm{FMR}}$, using 16 bins with a width of 0.04 dex. The metallicity dispersion is almost a Gaussian distribution, but with a noticeable tail towards lower metallicity values, as also noted in Mannucci et al. (2010) and Grønnow et al. (2015). We fit a Gaussian distribution function using least squares, which yields an offset $\mu = 0.009$ dex and a standard deviation $\sigma = 0.059$ dex, which is very similar to the observed values of $\sigma = 0.053$ dex and $\sigma = 0.048$ dex for SDSS galaxies found by Mannucci et al. (2010) and Grønnow et al. (2015), respectively. This shows that both observed and simulated galaxies exhibit a similar level of consistency with the evolution encoded in the FMR.

4.1 Distribution of mergers

Mannucci et al. (2010) proposed that strong low-metallicity gas inflows triggered during a merger are a plausible scenario to explain the tail of low-metallicity galaxies in the metallicity distribution. More recently, Grønnow et al. (2015) proposed a sophisticated model to infer different properties of mergers – merger ratios, metallicity dilutions, and characteristic timescales – from the distribution of residuals and the overabundance of outliers, showing also consistency with this scenario.

In order to study how merging galaxies are distributed with respect to the FMR, we opt to follow a different approach. Instead of trying to directly quantify the overabundance of outliers, which

strongly depends on the number of merging systems included in the sample, we calculate and compare the normalised distributions of residuals for isolated and merging galaxies. To do so the isolated phases of a galaxy are determined according to the sample in Section 2.3.

In the left-hand panel of Fig. 6, we show the normalized distribution of residuals. First, we note that merging galaxies exhibit a slightly higher probability to have lower than average metallicity values compared with their isolated counterparts. Moreover, they show a more distinct tail in the low-metallicity end, consistent with a merger-induced overabundance of outliers in the global distribution of residuals. The distribution of isolated galaxies also exhibits a somewhat smaller tail, which might be due to numerical issues related to our isolation criterion, or have a more physical origin; namely very minor mergers ($\mu < 1/100$), long post-merger transients, or cold gas accretion.

Finally, we test how different both distributions are. We compute the empirical distribution function (ECDF) in the right-hand panel of Fig. 6. Then, after applying a Kolmogorov–Smirnov test, we conclude that the null hypothesis of both distributions being numerical realizations drawn from the same underlying distribution can be rejected at a confidence level of $\alpha = 0.1$ per cent. This is good enough to affirm that the distributions are different and that isolated and merging galaxies follow different evolutionary paths in the SFR, $M_\star$ and Z_{gas} space. We thus confirm the result from Grønnow et al. (2015) that mergers cause outliers in the FMR.

4.2 Evolution of mergers: stacked profiles

After establishing that merging galaxies represent a distinct population with respect to the FMR, we explore how they are evolving out of and back into the isolated phases. In Fig. 7, we calculate the evolution of the fractional change of the SFR (top panels) and metallicity (bottom panels) for our merger sample. Each merger is normalized to its pre-merger values at $t_{\mathrm{SFR_{min}}}$ and $t_{Z_{\max}}$, respectively. The reference time is set to the coalescence time, with negative values corresponding to pre-merger stages.

In the central panels, we show the median of the stacked profiles, where the shaded regions represent 25–75 per cent percentile intervals. In the top-central panel we note that galaxies in a merger start experiencing a significant SFR-enhancement at around -0.3 Gyr, reaching a peak of 0.36 dex at coalescence and then decreasing again to pre-merger values. A closer inspection in the top-right panel, where we use three different mass ratio bins corresponding to major, intermediate, and minor mergers, shows that this evolution is mass-ratio dependent. For example, the SFR-peak values are 0.79 dex, 0.54 dex, and 0.18 dex for each respective bin, and they all occur at coalescence time. This result is expected given the correlations presented in Fig. 3, and also applies to the strongest metallicity dilutions seen in the bottom-central panel.

A second interesting aspect is the characteristic time-scale of the enhancement. Major mergers start the SFR-enhancement period at around -0.3 Gyr up to 0.7 Gyr, i.e. over a time-scale of 1 Gyr. For intermediate and minor mergers, this period goes from -0.3 Gyr to 0.5 Gyr, and from -0.2 Gyr up to 0.2 Gyr, respectively.

Now we calculate the distributions of the fractional change for the simulated and the FMR-predicted metallicities. The latter is computed from the stellar mass and the SFR of each merger along with the FMR of equation (2). In the bottom-central panel, we see that overall the metallicity is increasing in time due to the secular evolution of the galaxy. An exception to this occurs around the coalescence time, where significant dilutions of 0.08 dex and 0.025
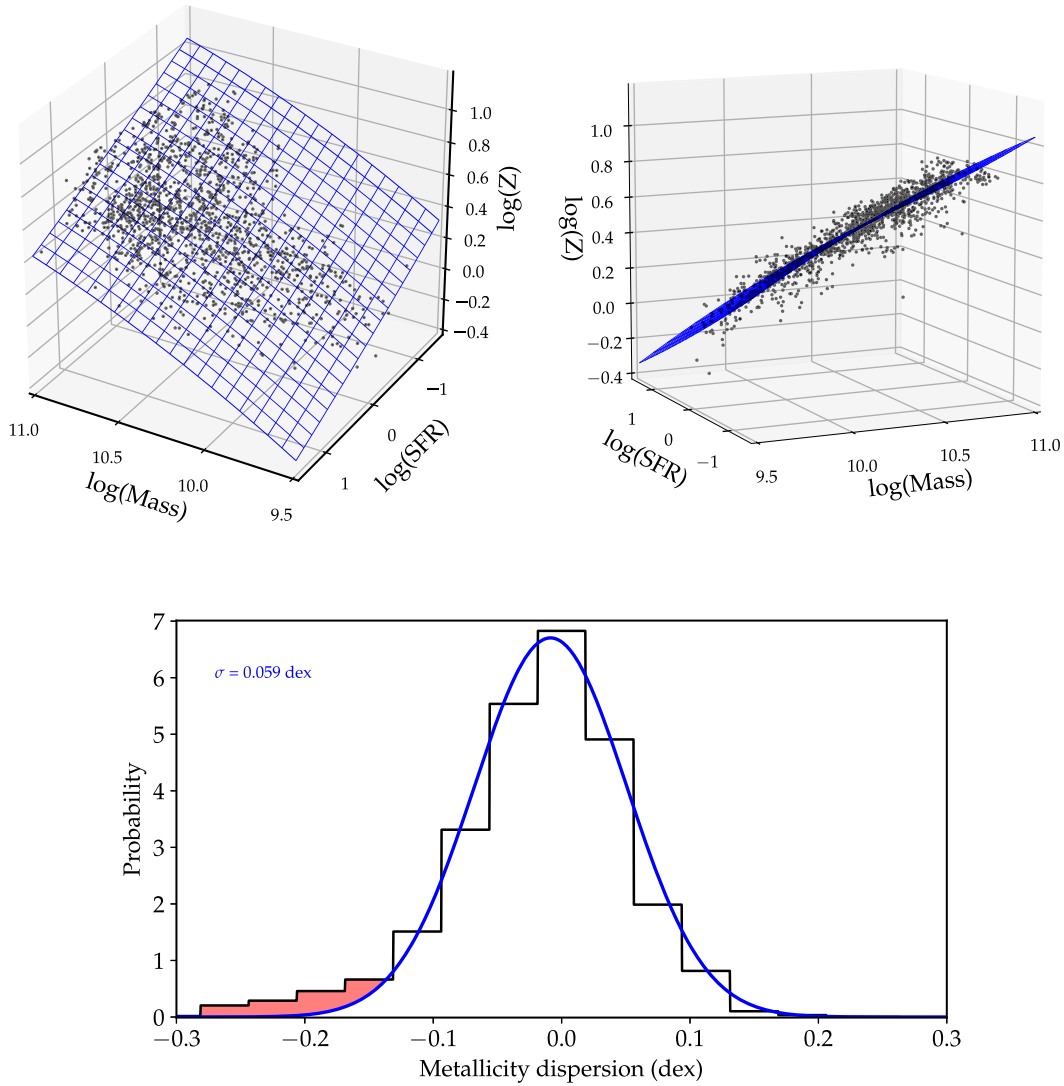
Figure 5. *Top panels:* two projections of the distribution of simulated galaxies at different times in the three-dimensional space of stellar mass–SFR–metallicity. The blue wireframe shows a second-order polynomial fitted to the data. *Bottom panel:* Normalized histogram of residuals around the fitted surface. We highlight the overabundance of low-metallicity outliers with a red shaded region. The blue line corresponds to a fitted Gaussian distribution function. The dispersion is similar to the value $\sigma = 0.053$ dex found by Mannucci et al. (2010) for their galaxy sample, which indicates a similar level of consistency of our simulated galaxies with an FMR.

dex are registered in the simulated and the FMR-predicted distributions, respectively. The FMR-predicted decrease is caused because the merging SFR-enhanced galaxies naturally yield lower metallicities in the FMR relation. However, this dilution is smaller than the simulated value, thereby confirming once more that merging galaxies consist of a differentiated population.

It is interesting to note that when we look at both distributions at more distant times from coalescence, i.e. for pre- and post-merger stages, they are more similar, meaning that the evolution is again well described by the FMR. This has the interesting consequence that a direct comparison can hint when the onset and the end of the dilution take place. In the bottom-right panel we show the dilution for the different mass ratio bins. For major mergers, we find that the onset of the dilution occurs at −0.4 Gyr, i.e. 0.1 Gyr before the onset of the SFR-enhancement. A time delay of 0.15 Gyr is also seen between the strongest metallicity dilution and the SFR-peak. In general, this is consistent with the results presented in Fig. 4 for metallicity versus distance projection, for which the dilution

starts to be significant at slightly larger distances than the SFR-enhancement. The dilution ends shortly after coalescence at 0.2 Gyr, while the SFR-enhancement is still significantly high. About 0.5-0.7 Gyr after the end of the dilution, the SFR reaches pre-merger values and the enhancement is over. During this period of time, the stellar enrichment is able to compensate the inflow of low-metallicity gas, placing the metallicity again close to the FMR-prediction.

For smaller merger ratios the metallicity dilution occurs at nearly similar times as the SFR-enhancement, with both having almost the same time-scales (see also Torrey et al. 2017a). This implies that the stellar enrichment from SF activity is less efficient at compensating gas inflows than in major mergers, and the dilution only ends when the infalling gas supply is dimmed after the merger process is completed.

Metallicity dilution and SFR-enhancement time-scales have been previously reported in hydrodynamical simulations of merging galaxies by Montuori et al. (2010). They study 1:1 gas rich mergers
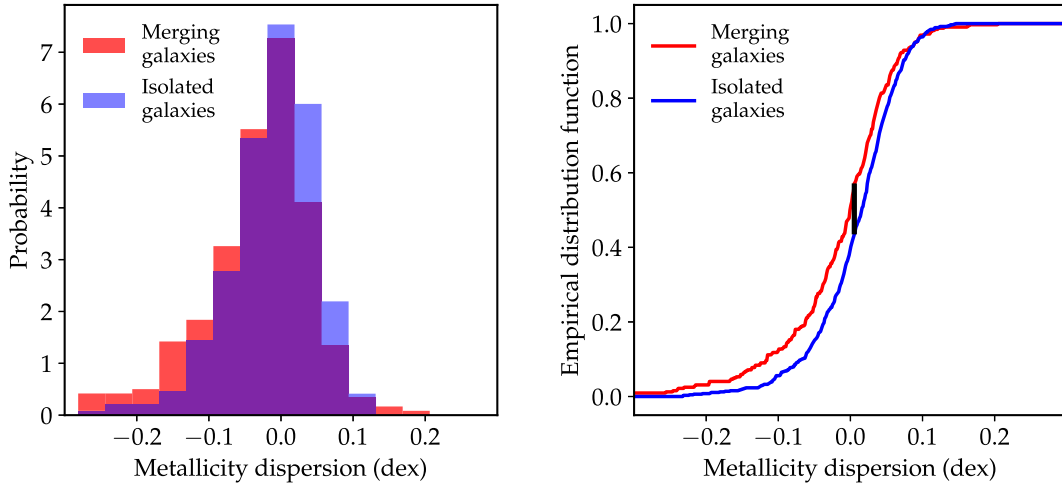
Figure 6. *Left–hand panel:* Normalized distributions of residuals of isolated galaxies (blue) and merging galaxies (red) with respect to the FMR. Merging galaxies have a more distinct tail towards low metallicities than isolated galaxies. *Right-hand panel:* Empirical cumulative distribution functions for isolated and merging galaxies. Applying a Kolmogorov–Smirnov test, both distributions differ at a confidence level of $\alpha = 0.1$ per cent, which is good enough to affirm that isolated and merging galaxies follow different evolutionary trends.
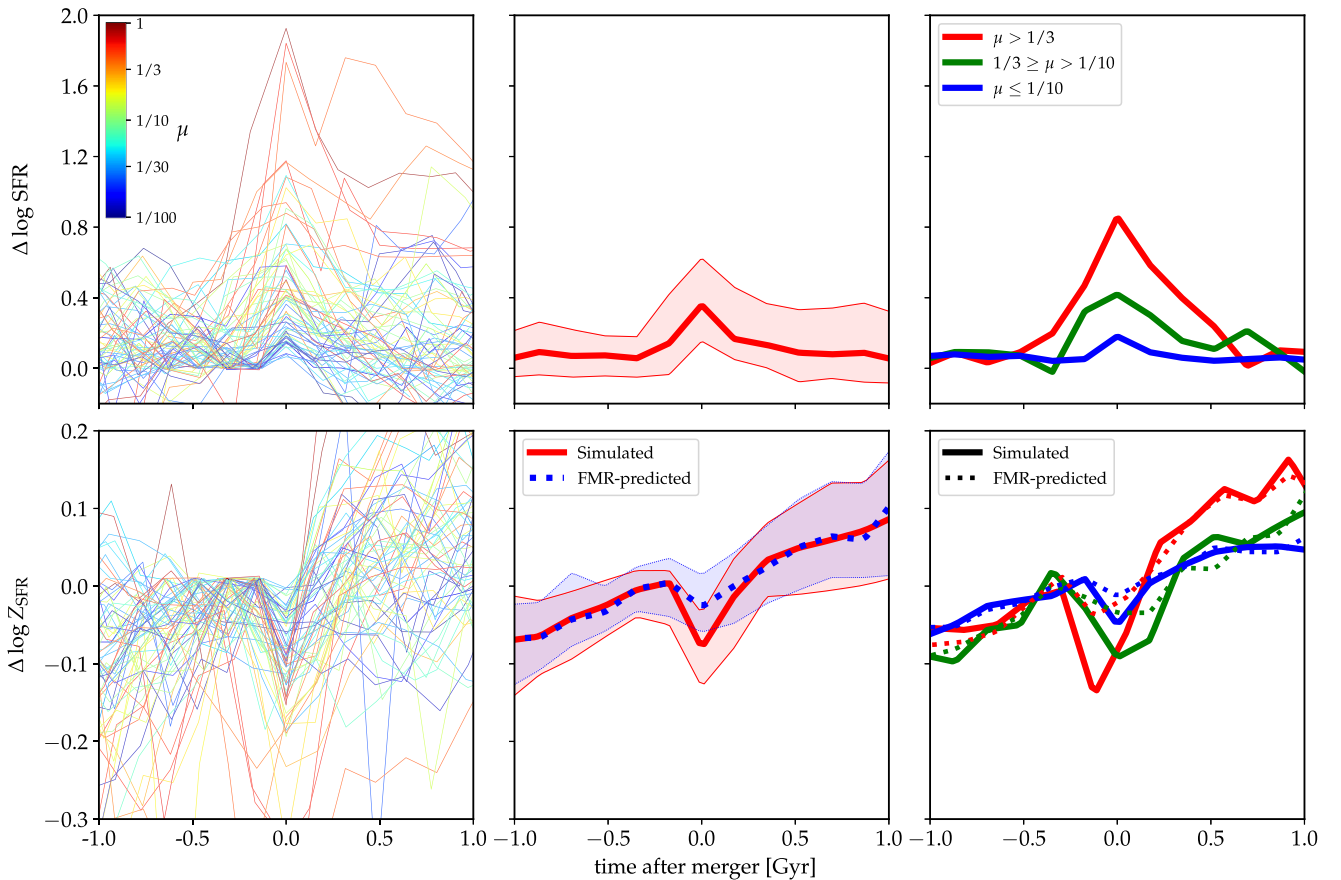
Figure 7. Fractional changes of the SFR (top-left panel) and metallicity (bottom-left panel) for the merger sample. Each merger is normalized to its pre-merger values at $t_{SFR_{min}}$ and $t_{Z_{max}}$, respectively. The x-axis shows the elapsed time since coalescence, with negative values corresponding to pre-merger stages. In the central panels we show the median of the stacked profiles, where the shaded regions correspond to 25–75 per cent percentiles. In the right panels, we show the median fractional changes for three different mass ratio bins, namely major (red), intermediate (green), and minor mergers (blue). For the metallicity, we compute the simulated and the FMR-predicted values. The latter is computed from the stellar mass and the SFR of each galaxy along with the fitted FMR of equation (2). Close to coalescence, we note that the simulated metallicity is always lower than the FMR prediction.

and find a time-scale of 1.5 Gyr for both processes. Our SFR-enhancement time-scale of 1 Gyr for major mergers is consistent with their result, although our dilution time-scale is considerably shorter. A plausible explanation for this discrepancy is that their galaxies are more gas-rich, with gas fractions of 20 per cent compared to $9 - 16$ per cent for our galaxies. This, along with the higher mass ratio, might cause significantly stronger low-metal gas inflows in their simulations, hence the stellar enrichment during the SFR-enhancement cannot overcome the dilution, resulting in both processes having similar time-scales.

5 DISCUSSION

Based on idealized merger simulations where two composite model galaxies collide on a Keplerian orbit, it has previously been suggested that *wet mergers* can be sensibly divided into two categories; minor and major mergers. The merger mass ratios defining these two classes are typically taken to be $1/10 < \mu < 1/3$ and $\mu > 1/3$, respectively. The former mass-ratio reflects the limit below which a negligible SFR-enhancement arises, and the latter reflects the threshold above which a strong SFR-peak occurs. Furthermore, it has been established that major mergers also consume their gas on shorter time-scales than minor mergers (e.g. Cox et al. 2008). In our cosmological simulations, we confirm that stronger SFR-peaks and shorter gas consumption time-scales occur for major mergers compared to minor mergers. We additionally show that a strong metallicity dilution occurs for major mergers, whereas for minor mergers the effect is more modest. We advocate that merger-induced metallicity dilution is an important addition to the standard picture of the behaviour of wet mergers. Aside from our own simulations, this is also supported by those of Torrey et al. (2012a) and Torrey et al. (2017b). Furthermore, this effect is seen in the observations of Scudder et al. (2012).

Observers have for more than half a decade advocated the existence of the FMR, and recently several hydrodynamical galaxy formation simulations have reproduced this relation (Lagos et al. 2016; De Rossi et al. 2017; Davé et al. 2017; Torrey et al. 2017a). The effect of merger-induced metallicity dilution has important consequences for the FMR, because mergers are expected to produce a low-metallicity tail in the residuals around the FMR. This result has been seen in analysis of the observations of Grønnow et al. (2015) and is also visible in our simulations.

In this paper, we have focused on the effect of gas flows in the central parts of galaxies. Several questions which can be addressed in future research arise from this work. It would, for example, be interesting to study gas flows by using *Lagrangian gas tracer particles* (for a study of gas tracers within our simulation framework, see Genel et al. 2013) to quantify how the gas is redistributed within a galaxy in a merger. This would specifically make it possible to estimate to what extent gas is moved between the core of a galaxy, the disk, and the circumgalactic medium. Furthermore, it would be possible to study gas accretion from outside the galaxy in detail. In our current set of merger simulations, we have not included such gas tracer particles, but in future simulations we plan to do so.

6 CONCLUSION

In this paper, we study cosmological simulations of *wet mergers* of main progenitor galaxies with masses in the range $5 \times 10^9 \, \mathrm{M_\odot} < M_* < 2 \times 10^{11} \, \mathrm{M_\odot}$ from the Auriga simulation suite. Our sample of mergers is much larger than what has been typically used in studies of idealized merger simulations, and with our full cosmological

setup we furthermore have more realistic structure, encounter orbits, and environment of our galaxies. Our main results are:

(i) We confirm the result from idealized simulations that strong starbursts occur in major mergers with a mass-ratio larger than $\mu > 1/3$. For minor mergers with $1/10 < \mu < 1/3$, there is typically a smaller, but still clearly visible SFR enhancement. Exceptions do, however, occur when several galaxies are involved in the minor merger; in this case, the SFR can also increase by an order of magnitude. We note that this scenario, which happens at least occasionally for galaxies in the real Universe, has not been properly explored in previous generations of idealized merger simulations.

(ii) An increased merger ratio also causes a shorter gas consumption timescale, i.e. more bursty star formation. We furthermore find that a low-metallicity epoch is typically associated with a merger. The magnitude of the metallicity dilution is strongest for major mergers. Our cosmological simulations thus confirm the occurrence of metallicity dilution, which has previously been seen in observations of merging galaxies and in idealized merger simulations. We consider the period of metallicity dilution as an equally characteristic feature of major mergers as the increased SFR and decreased gas consumption time-scale.

(iii) During the epoch of metallicity dilution, mergers have lower metallicity than predicted by the *fundamental metallicity relation* (FMR). This creates a tail of low-metallicity galaxies offset from the FMR. Consistent with findings for observed galaxies, the residuals around the FMR indicate that there are more galaxies with low metallicity than predicted by a Gaussian distribution of the residuals. At least part of this effect can be attributed to galaxy mergers.

REFERENCES

Barnes J. E., 2004, MNRAS, 350, 798
Belli S., Jones T., Ellis R. S., Richard J., 2013, ApJ, 772, 141
Brown J. S., Martini P., Andrews B. H., 2016, MNRAS, 458, 1529
Chabrier G., 2003, PASP, 115, 763
Christensen L. et al., 2012, MNRAS, 427, 1953
Cortijo-Ferrero C. et al., 2017, MNRAS, 467, 3898
Cox T. J., Jonsson P., Somerville R. S., Primack J. R., Dekel A., 2008, MNRAS, 384, 386
Daddi E. et al., 2010, ApJ, 714, L118
Davé R., Rafieferantsoa M. H., Thompson R. J., Hopkins P. F., 2017, MNRAS, 467, 115

Dayal P., Ferrara A., Dunlop J. S., 2013, MNRAS, 430, 2891

De Rossi M. E., Bower R. G., Font A. S., Schaye J., Theuns T., 2017, MNRAS, 472, 3354

Di Matteo P., Bournaud F., Martig M., Combes F., Melchior A.-L., Semelin B., 2008, A&A, 492, 31

Ellison S. L., Patton D. R., Simard L., McConnachie A. W., 2008a, ApJ, 672, L107

Ellison S. L., Patton D. R., Simard L., McConnachie A. W., 2008b, AJ, 135, 1877

Gabor J. M., Capelo P. R., Volonteri M., Bournaud F., Bellovary J., Governato F., Quinn T., 2016, A&A, 592, A62

Genel S., Vogelsberger M., Nelson D., Sijacki D., Springel V., Hernquist L., 2013, MNRAS, 435, 1426

Grand R. J. J. et al., 2017, MNRAS, 467, 179

Grand R. J. J., Springel V., Gómez F. A., Marinacci F., Pakmor R., Campbell D. J. R., Jenkins A., 2016, MNRAS, 459, 199

Grasshorn Gebhardt H. S., Zeimann G. R., Ciardullo R., Gronwall C., Hagen A., Bridge J. S., Schneider D. P., Trump J. R., 2016, ApJ, 817, 10

Grønnow A. E., Finlator K., Christensen L., 2015, MNRAS, 451, 4005

Hayward C. C., Torrey P., Springel V., Hernquist L., Vogelsberger M., 2014, MNRAS, 442, 1992

Hopkins P. F., Cox T. J., Hernquist L., Narayanan D., Hayward C. C., Murray N., 2013, MNRAS, 430, 1901

Hunter J. D., 2007, Computing In Science & Engineering, 9, 90

Karakas A. I., 2010, MNRAS, 403, 1413

Karman W., Macciò A. V., Kannan R., Moster B. P., Somerville R. S., 2015, MNRAS, 452, 2984

Kewley L. J., Rupke D., Zahid H. J., Geller M. J., Barton E. J., 2010, ApJ, 721, L48

Krumholz M. R., Dekel A., McKee C. F., 2012, ApJ, 745, 69

Lagos C. d. P. et al., 2016, MNRAS, 459, 2632

Lara-López M. A. et al., 2010, A&A, 521, L53

Lotz J. M., Jonsson P., Cox T. J., Primack J. R., 2008, MNRAS, 391, 1137

Mannucci F., Cresci G., Maiolino R., Marconi A., Gnerucci A., 2010, MNRAS, 408, 2115

Marinacci F., Pakmor R., Springel V., 2014, MNRAS, 437, 1750

Martig M., Bournaud F., 2008, MNRAS, 385, L38

Mihos J. C., Hernquist L., 1996, ApJ, 464, 641

Montuori M., Di Matteo P., Lehnert M. D., Combes F., Semelin B., 2010, A&A, 518, A56

Moreno J., Torrey P., Ellison S. L., Patton D. R., Bluck A. F. L., Bansal G., Hernquist L., 2015, MNRAS, 448, 1107

Moster B. P., Macciò A. V., Somerville R. S., Naab T., Cox T. J., 2011, MNRAS, 415, 3750

Pakmor R., Springel V., Bauer A., Mocz P., Munoz D. J., Ohlmann S. T., Schaal K., Zhu C., 2016, MNRAS, 455, 1134

Patton D. R., Torrey P., Ellison S. L., Mendel J. T., Scudder J. M., 2013, MNRAS, 433, L59

Perez F., Granger B. E., 2007, Computing In Science & Engineering, 9, 21

Perez J., Michel-Dansac L., Tissera P. B., 2011, MNRAS, 417, 580

Planck Collaboration et al., 2014, A&A, 571, A16

Renaud F., Bournaud F., Kraljic K., Duc P.-A., 2014, MNRAS, 442, L33

Rodriguez-Gomez V. et al., 2015, MNRAS, 449, 49

Rupke D. S. N., Kewley L. J., Chien L.-H., 2010, ApJ, 723, 1255

Salim S., Lee J. C., Davé R., Dickinson M., 2015, ApJ, 808, 25

Sanders R. L. et al., 2018, ApJ, 858, 99

Sanders D. B., Scoville N. Z., Soifer B. T., 1991, ApJ, 370, 158

Schaye J. et al., 2015, MNRAS, 446, 521

Scoville N. Z., 2013, Evolution of star formation and gas. Cambridge Univ. Press, p. 491

Scudder J. M., Ellison S. L., Torrey P., Patton D. R., Mendel J. T., 2012, MNRAS, 426, 549

Sparre M., Springel V., 2016, MNRAS, 462, 2418

Sparre M., Springel V., 2017, MNRAS, 470, 3946

Springel V. et al., 2005, Nature, 435, 629

Springel V., 2010, MNRAS, 401, 791

Springel V., Hernquist L., 2003, MNRAS, 339, 289

Springel V., Di Matteo T., Hernquist L., 2005, MNRAS, 361, 776

Stott J. P. et al., 2013, MNRAS, 436, 1130

Teyssier R., Chapon D., Bournaud F., 2010, ApJ, 720, L149

Thielemann F.-K. et al., 2003, Nucl. Phys. A, 718, 139

Torrey P. et al., 2017a, MNRAS, 477, L16

Torrey P. et al., 2017b, preprint (arXiv:1711.05261)

Torrey P., Cox T. J., Kewley L., Hernquist L., 2012a, ApJ, 746, 108

Torrey P., Vogelsberger M., Sijacki D., Springel V., Hernquist L., 2012b, MNRAS, 427, 2224

Travaglio C., Hillebrandt W., Reinecke M., Thielemann F.-K., 2004, A&A, 425, 1029

Tremonti C. A. et al., 2004, ApJ, 613, 898

Van Der Walt S., Colbert S. C., Varoquaux G., 2011, Computing In Science & Engineering, 13, 22

Vogelsberger M., Genel S., Sijacki D., Torrey P., Springel V., Hernquist L., 2013, MNRAS, 436, 3031

Yabe K. et al., 2015, PASJ, 67, 102

This paper has been typeset from a TEX/LATEX file prepared by the author.